UCRL-ID-125461

# Electrical Impedance Tomography of the 1995 OGI Perchloroethelyne Release

W. Daily
A. Ramirez

October 1, 1996

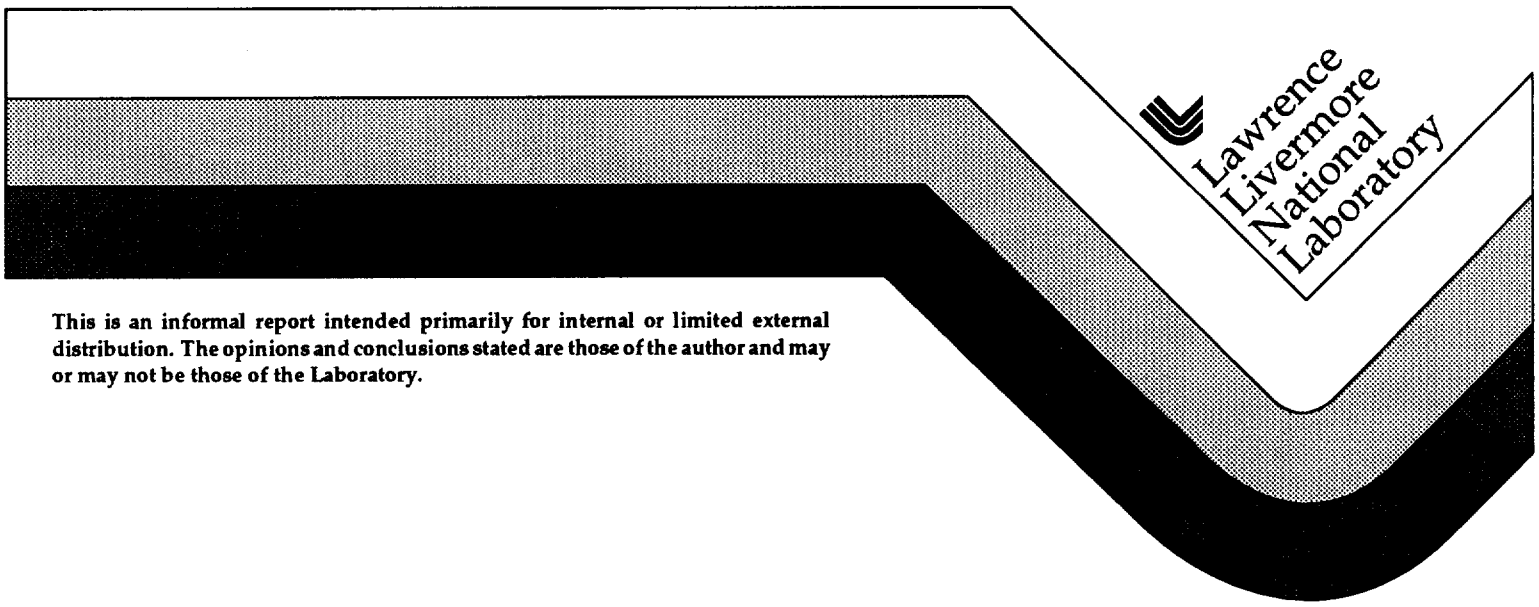

# Electrical Impedance Tomography of the 1995 OGI Perchloroethelyne Release

William Daily and Abelardo Ramirez
Lawrence Livermore National Laboratory
Livermore, CA 94550

October 1996

*Abstract-*

The goal of this work is to determine if electrical impedance tomography (EIT) might be useful to map free product DNAPL contamination. EIT was used to image the plume resulting from a release of 189 liters (50 gallons) of perchloroethylene (PCE) into a saturated acquifer constructed of sand with two layers of bentonite. Images were made in 4 planes, before, during and after the release, to generate a detailed picture of the spatial and the temporal development of the plume.

For the first time, information of the electrical impedance (both in phase and out of phase voltages) was used at several different frequencies to produce images. We observed some frequency dispersion in the images before and after the PCE release. Some laboratory measurements of organic contamination in soil to indicate detectable dispersion
. A search for this effect in EIT images reveals weak evidence, the signal appearing just above the measurement uncertainty, of a change in the reactance (IP effect) in the soil because of the PCE.

## Background and Description of EIT

Contamination of soil and groundwater by organic compounds is one of our most serious environmental problems. Efficient and effective strategies can be designed for remediation only when the spatial extent of the contamination is well understood. The purpose of this work is to determine if electrical resistance tomography (ERT) or its generalization, electrical impedance tomography (EIT), can be used to map the spatial extent of free product, dense non-aqueous phase liquids (DNAPL) in the subsurface. Of particular importance is the ability to achieve such a map without the benefit of baseline data; the usual circumstance, where access to the contaminated soil is possible only after the fact.

The basis for achieving this goal is found in laboratory measurement of the electrical response of contaminated soil. Olhoeft (1986, 1992) and Trude *et al.* (1989) report that a toluene contaminated soil has a unique electrical dispersion, resulting from one or more clay-organic reactions. The hope is that this phenomenon might permit discrimination between contaminated and clean soil by comparing electrical phase measurements at two or more frequencies. Figure 1 shows that laboratory data for clean and contaminated soil from Olhoeft (1986). The observed increase in impedance magnitude is expected since the resistive DNAPL is displacing conductive pore water, however, the broad peak that appears in the phase response is unexpected (Figure 1).

Others have more recently reported a similar effect. Sadowski (1988) reports large changes in phase spectra near 50 Hz when montmorillonite samples were contaminated by toluene. Vanhala (1996) report that the complex resistivity of sand and till when contaminated with motor and waste oil has a characteristic convex upward phase response between 1 and 1000 Hz but is convex downward when clean. This behavior is reminiscent of the phase results reported by Olhoeft (1986). We conclude from the above mentioned work that laboratory evidence points to the possibility of a unique signature from organic contamination of a soil in the phase spectra of the complex resistivity between 1 and 1000 Hz.

Electrical impedance tomography (EIT) is a technique for reconstruction of subsurface electrical impedance (electrical resistance tomography, or ERT, if the ground is not reactive in nature). The result of such a reconstruction is a 2 or 3 dimensional map of the electrical impedance distribution underground made from a series of voltage and current measurements from buried electrodes. The EIT approach we follow here relies on detection and mapping of the changes in electrical impedance associated with a release of PCE. The technique of EIT has been used to map subsurface liquids during natural or man-induced processes and to map geologic structure. For example, man-induced processes such as tank leaks (Ramirez and Daily, 1996) and clean-up processes such as steam injection (Ramirez *et al.*, 1993), can create changes in a soil's electrical properties that are readily measured and imaged.

To do EIT surveys we place a number of electrodes in boreholes and/or at the ground surface to sample the subsurface impedance distribution using an automatic data collection and switching system.

A few hundred 4 electrode electrical impedance measurements are collected using of these electrodes. These data are processed to produce electrical tomographs using state of the art data inversion algorithms.

All previous imaging using galvanic currents has been using voltage measured in phase with the transmitted current. However, other options are also possible. Consider the simplest of electrical circuits in which the voltage drop across a resistor is in phase with the current flowing through the resistor. For this case the ratio of the instantaneous voltage and current is a constant called resistance, $\rho$ and is called Ohm's law . In general, however, the voltage and current will not be synchronous. In this case, they are represented as complex quantities, wherein Ohm's law still applies but yields a complex quantity, impedance $z = \rho + i\nu$ where $i = (-1)^{1/2}$. If the current phase leads the voltage phase then z is called capacitive and if the current lags the voltage it is called inductive (these terms arising from the behavior of lumped circuits of capacitors and inductors).

Not only is impedance is a complex quantity, it may also vary with frequency--a property called dispersion. We will present images inverted from measurements at various frequencies to indicate any electrical dispersion which might be present in the subsurface.

## Description of 2D Algorithm

Here we describe briefly some of the important features of the 2D algorithm. For additional details, the reader is referred to LaBrecque et al. (1996). The algorithm solves both the forward and inverse problems. The forward problem is solved using a finite element technique. The algorithm implements a regularized solution which minimizes an objective function. The objective of the inverse routine is to minimize the misfit between the forward modeling data and the field data, and a stabilizing functional of the parameters. The stabilizing functional is the solution's roughness. This means that the inverse procedure tries to find the smoothest resistivity model which fits the field data to a prescribed tolerance.

## Experimental Setup

## Data Acquisition System

ZOMBIE, our unique data acquisition system, has four basic components: transmitter or current source; receiver which measures the transmitted current as well as the resulting electrode potentials; multiplexer for connecting the electrodes to the transmitter and receiver; a computer for system control and data archival. A block diagram of the system is shown in Figure 2. We now summarize the capabilities of each of these components:

*Transmitter*

The current source is powered by a 125 volt, 400 Hz generator. The output square wave is synchronized between 0.0007 Hz and 8 k Hz with the receiver by an electrically isolated connection or by an internal crystal clock. The output can be regulated to either constant current or constant voltage for a maximum of 3 k watts output.

*Receiver*

The heart of the system is a multichannel detector capable of supporting up to 16 modular detectors, each with a10 M ohm input impedance at DC, a 16-bit A/D converter and a dynamic range from ±0.03 μv to ±32v. This large dynamic range is an important attribute when acquiring EIT data since electrode combinations are used in imaging which yield a large variation in received voltage. There is an automatic SP offset adjustment of up to ±2.25 V in 65μ V steps. Each channel has automatic gain setting in binary steps from 1 to 65,536, but a with manual override the gains may be set externally--a time saving feature when high data rates are needed. Calibration of each channel can be accomplished against either an internal or externally supplied reference voltage.

In practice one channel is used to measure the transmitted current as a voltage drop across a calibrated resistor in the transmitter circuit. This leaves 15 channels for simultaneous potential measurements and is a major reason for the increase in data acquisition rate of ZOMBIE over most other instruments which are single channel.

The receiver operates in both the frequency domain and time domain. Twenty four frequencies can be selected in binary intervals between 0.0007 Hz and 8 k Hz and over this range both the signal magnitude and phase can be measured.

*Multiplexer*

Inherent in the switching scheme is the use of "dumb" electrodes. This means that the switching is accomplished at a central point and is not distributed to the individual electrode positions as in many "smart" electrode systems. "Dumb" electrodes require that a separate wire connect the central switching bank (multiplexer) and each electrode. Although this requires more wire and sometimes more field set up time, it makes for disposable electrodes--the only type which can be grouted into boreholes in any significant number at reasonable cost. Since our strategy is to position electrodes underground, as close as possible to the imaged region, ZOMBIE requires "dumb" electrodes with a central multiplexer.

The multiplexier system is modular. Each module can address 30 separate "dumb" electrodes and modules can be daisy-chained together to handle multiples of 30 electrodes. Control of each module is via RS232 protocol such that any electrode can be connected to either high or low side of the current source or the high or low side of any detector. Contributing to the overall system data acquisition rate is the switching speed which is 100 ms. The multiplexer switches are rated at 10 amperes and 500 volts.

*Computer*

System control is via RS232 protocol from a notebook computer to the receiver and multiplexer. The control software is written in a graphical interface language which is very user friendly.

All of the essential front panel controls on the receiver can be set remotely via the RS232 link: time domain or frequency domain operation, source frequency, stacking, analog stage power line filters, and amplifier gains. Data is downloaded in real time from the receiver to the computer and displayed so that the operator can easily monitor data acquisition.

The multiplexer control allows for complete freedom in specifying which electrodes are used for current source and which are used for potential measurement. This protocol is specified by the user in an ASCII file read by the control program.

**System performance**

The following summary of system performance is drawn from experience during the work reported herein and from laboratory tests

*Data acquisition speed*
Data rates are determined by the number of channels which could be continuously used, source frequency and staking requirements. Under normal conditions, at 64 Hz and staking for 1 sec, it is possible to acquire data with about 1% error in the magnitude (as determined by comparing reciprocal measurements) at a rate of 3077 transfer resistance measurements per hour (mph). This data rate could be increased by pre measuring the analog amplifier gains for each measurement and using these gain settings instead of allowing the system to determine them before each measurement. Using prerecorded gains the data rate increases to about 4000 mph.

*Data accuracy*
Accuracy is usually defined as "the conformity of an indicated value to an accepted standard value, or true value" (precision, on the other hand, is the "degree of exactness with which a quantity is stated") (Considine, 1983). As one measure of system accuracy we have performed a simple system calibration against a NIST standard. One channel was used to measure the current through a standard resistor (with a NIST pedigree) while another channel was used to measure the resulting potential drop. Calibration is typically accurate to better than 1%. This is a check of the routine field calibration.

Unfortunately, this calibration is only a lower limit of the errors in field data where electrode noise, cable coupling, external noise sources, etc. will combine to increase the errors and decrease accuracy. Maximizing data accuracy on a system where errors may vary from one electrode pair to another, or even change with time, is a difficult problem. Equally important, but just as difficult to obtain, is a reliable *measure* of accuracy since fitting the forward model calculations to the measured data to an arbitrarily close tolerance can lead to obviously incorrect inversions (see LaBrecque *et al.*, 1996). Clearly, data accuracy and estimates of that accuracy are important factors in determining overall image quality.

Several measures are used to estimate data accuracy. The most common is repeatability but our experience has been that this test leads to a serious underestimate of error. We have found that reciprocity is a better estimate of error (for a normal 4 electrode measurement of transfer resistance, the reciprocal is found by interchanging the current source and potential measurement electrodes).

The actual resistance magnitude errors estimated using this method are dominated by sources other than the data acquisition electronics: electrode material, formation resistivity, formation electrochemistry, ambient electromagnetic noise, etc. By comparing each datum with its reciprocal we estimate the errors in resistance magnitude typically between about 1 and 10% and showing a weak correlation with the transfer resistance magnitude.

To estimate errors in phase of individual voltage measurements we studied the instrumental response to a purely resistive load at a fixed frequency. We find that at 1 Hz the errors are a few m rad but increase rapidly with increasing frequency. In fact, at 256 Hz the errors are typically few 10s of m rad. The source of this error is unknown but it is known to be a function of the signal amplitude. For example, at 256 Hz, between about 50 mV and 3 V, the error is 20 m rad but below 50 mV it be as high as 70 m rad. From the laboratory data of complex resistivity of soils (e.g., Olhoeft, 1986) this error is the same order as the expected signal.

*Test of System Performance*

A simple test of the measurement system was devised using a network of resistors shown in Figure 3. Each resistor junction on the periphery was used as a current injection or potential measurement point (electrode position) and then complex resistivity data (magnitude and phase) was taken at 1 and 256 Hz for both the case without the four 1 μF capacitors shown and with them as shown in the figure. In both cases we have reconstructed the quantity

$$(|X\,(f = 256)|\,/|X\,(f = 1)|)\,R_{h,DC} \qquad (6)$$

where $X\,(f = 256)$ is the transfer resistance measured at 256 Hz, $X\,(f = 1)$ is the transfer resistance measured at 1 Hz and $R_{h,DC}$ is the transfer resistance magnitude calculated for a uniformly resistive mesh of 1 ohm m assuming quasi static conditions.

For the case without the capacitors we recover an image of 1 ohm m with variations of about 12 % which is the variability manifest in the reconstruction due to both experimental error in the data and numerical instability in the inversion. For this network (carbon resistors were used to minimize inductance of wire wound resistors) the impedance is purely resistive; there is no indication of a

capacitive reactance which would be manifest as a systematic dispersion in the reactance with frequency.

On the other hand, for the case with four capacitors in the network as shown in Figure 2 we recover an image of 1 ohm m with approximately 50% depression centered on the element containing the capacitive reactance. The reactance of each capacitor is $1/i\,\omega C$ where $\omega$ is the angular frequency and C is the capacitance so that the impedance of each resistor, r, and capacitor in parallel is

$$1/X = [1/r] + [1/(1/i\,\omega C)] \qquad (7)$$

so that the impedance magnitude is

$$|X| = \{r^2 + (1/\omega C)^2\} \,/\, \{(1/r\omega C) + r\omega C\}^2 \qquad (8)$$

For a 1 K ohm resistor and 1 $\mu$F capacitor at 1 Hz $|X| = 900$ ohms but at 256 Hz $|X| = 520$ ohms which is a 42% drop in the impedance magnitude which agrees reasonably well with the 50% change in resistance shown in Figure 2.

The basis of induced polarization is the frequency dependence of complex resistivity. One description of induced polarization is the frequency effect (FE) (Parasnis, 1966 and Borner *et al.*, 1996) which is the fractional change in impedance magnitude with frequency

$$FE = \{|X(\omega_1)| - |X(\omega_2)|\}/|X(\omega_2)| \qquad (9)$$

This quantity is a convenient way of determining the electrical behavior of the rock since using a simple constant phase angle model (Borner *et al.*, 1996) it is possible to relate FE and the phase angle. It can be particularly important since the magnitude can be more accurately measured than phase. In our data the phase errors, estimated from reciprocity, are about 20% at 256 Hz, whereas the magnitude errors are 4% at the same frequency. For this reason, in the next section we will use the concepts of FE to investigate the reactive behavior in the experimental data.

**Field experiment set up**

The experiment was conducted in a double wall steel tank 10 meters square and 5 m deep at the Oregon Graduate Institute of Science and

Technology in Beaverton, Oregon. This tank was then lined with an impermeable geomembrane liner and this construction to allow the safe release of PCE into a soil section constructed of sand and clay. Dune sand from a nearby quarry was placed in the tank with no special efforts at consolidation or layering. However, two layers of powdered bentonite were included as shown in Figure 4. The top layer was about 7 cm thick powdered bentonite. The lower layer was planned to be two layers; the lower 7 cm powdered bentonite and directly above that a 25 cm mixture of1% bentonite and sand. However, it was difficult constructing this slurry on top of the dry layer without mixing of the two. The lower layer is likely a heterogeneous mixture about 30 cm thick of the slurry and the pure clay. We also found it difficult to install either the half upper layer or the full lower layer without some mixing with the sand above and below. Despite these difficulties both confining layers are approximately as planned and functioned pretty much as expected.

The tank was saturated with 4 ohm m pore water to within about 25 cm of the surface. Our intent was to release the PCE at the surface above the edge of the upper bentonite layer and image the downward growth of the plume, its interaction with the upper layer, its continued drop to the lower layer and its residence on the lower layer.

A total of six electrode arrays were used to generate two dimensional (2D) images in four planes. The arrangement allows for one long cross section through the tank using the coplanar arrays L1, L2, L3 and L4 while arrays L5 and L6 were used to produce an image plane perpendicular to that section (see Figure 3). Each array contained 10 lead electrodes spaced evenly between 50 cm and 275 cm depth. During construction, each array was supported within the tank while the sand and bentonite were placed at each level. This minimized any vertical migration path the arrays might provide, especially through the clay.

Twelve other boreholes were installed in the tank, each constructed of glass casing 10.2 cm diameter and extending 2.34 m deep. From these wells it was possible to use a special video camera to identify the PCE which was dyed red. The glass boreholes were also used to acquire thermal neutron absorption data using a conventional soil moisture probe.

One hundred eighty nine liters (50 gallons) of perchloroetheylene (PCE, dyed red using floricyne to facilitate identification using the downhole video camera) was released at a single point on the surface approximately midway between arrays L2 and L3. The release rate averaged about 2.0 liters/hr. The phreatic surface was at about 25 cm depth during the entire experiment although it did change some with added water during rain and evaporation during fair weather.

EIT data was collected, usually each day, at 1, 64, 256, 512 and 1024 Hz between planes L1-L2, L2-L3, L3-L4 and L5-L6. Baseline data, four complete sets during the release, and eight data sets after the release ended, amounted to 4,400 transfer impedances measured each day or more than 57,000 measurements over the course of the experiment. The magnitude of these combined data files underscores two points. First, automated high speed data acquisition was essential for success of the project. Second, each reconstructed image discussed in the next section represent several hundred data and therefore a high information density.

## Results and Discussion

### EIT of DNAPL using baseline data

Reconstructions will be displayed with planes L1-L2-L3-L4 in one panel representing a section through the tank 3 m long and 2.25 m high. Plane L5-L6 is not shown.

The baseline image at 1 Hz is shown in Figure 4. The resistivity, varies between $10^0$ and $10^3$ ohm m with the full clay layer at 2 m and the half layer at 1.2 m imaged at the low values and the sand at the high end of the scale. The intent was to construct a section with typical electrical properties. These resistivity values are not unusual for natural soils in the western U.S.

The right parts of plane L2-L3 and L3-L4 are more resistive, probably as a result of heterogeneity in the sand. Another resistive zone appears lower in plane L3-L4 above the lower clay. Both bentonite layers are clearly imaged, the upper extending only part way across the tank. They are also clearly not uniform; the blochyness of the layers reflects the difficulties installing these structures in the tank as well as imperfections in the inverse process. The section also shows that the upper layer does not extend to the center of the L2-L3 plane as planned. This may be an artifact of the inversion algorithm because of the very high electrical contrast

between the clay and sand. We shall see later that the PCE plume moves around the end of this layer in a manner consistent with it extending to the middle of L2-L3 plane. EIT gives a detailed sectional view of variability in these confining layers which is impossible to achieve with conventional logging or even surface radar methods.

Data for the baseline images in Figure 4 were acquired the morning of August 16, 1995. The PCE release began at 1300 hours the same day at a rate of 2.0 liters/hr and then another EIT data set was taken for all planes after about 7 liters had been released. The panels in Figure 5 show those reconstructions after a pixel by pixel subtraction of the background images and therefore show only changes in resistivity distribution. At 3.5 hours the changes were quite small but the most significant feature is located below the release point--a resistive anomaly arching around the end of the upper clay. This anomaly probably forms as the resistive PCE displaces the more conductive pore water. Other small anomalies in this image are probably from unrelated but natural changes in the pore water conductivity and data noise. As we pointed out earlier, the arching anomaly associated with the plume moving around the upper clay layer is consistent with that layer extending all the way to the center of plane L2-L3 even though it appears truncated in the tomograph of Figure 3.

The next data, on August 17 about 21 hours and 42 liters into the release, clearly shows that the anomaly has grown large enough to extend from the release point, arch around the upper clay and reach down to just touch the lower confining layer. Apparently, most of the PCE continues to spill over the edge of the upper layer with little residing on top. Reflecting the dynamic nature of the system, the same small unrelated anomalies are still present and now a few others are forming. The weak disconnected features forming along the top of the lower clay may be small accumulations of PCE even at this early stage.

By August 18, the anomaly begins to spread horizontally along the top of the lower clay as might be expected of the plume as it reaches that confining layer. The appendage pointing up to the right in plane L2-L3 is not expected and we cannot explain its presence.

The release ended Sunday at noon, August 20 after 189 liters (50 gallons) was released. On Monday, August 21 the tomographs show a

different picture from that 3 days earlier. Only a small remnant is left of the arching anomaly from the surface and around the upper clay. This is understandable if it represented the downward moving PCE which by this time has mostly drained and been replaced by water. However, now a resistive anomaly almost 2 m long sits at the top of the lower clay layer, centered directly below the edge of the upper layer. From this tomograph we conclude that the bulk of the PCE has drained from the sands and is pooled on the lower layer. A 2 m diameter pool of 6 cm uniform thickness would accommodate the volume released and so the anomalies are consistent with a PCE pool at this location. However, the images imply a non uniform free product pool. The data suggest a free product pool the distribution of which is determined by non uniformity in the confining boundary.

Difference images were also constructed for 4, 16 and 25 days after the release ended. In these images there are two clear trends. First, the anomaly associated with the free product plume breaks apart into separate pieces and each part becomes weaker with time. One explanation is that the free product is moving into topographically lower regions of the clay surface which are out of the image plane. The tomographs on August 24 suggest another possibility--that PCE is moving downward, perhaps along array L3, through the lower clay layer. The second trend is that anomalies unrelated to the PCE release are becoming more important. Especially prominent are those at the top right in the image planes. These may be due to the addition of fresh pore water to the tank as a result of heavy rains on September 5.

**Comparison of EIT, neutron logs and video logs**

Two data sets, independent of EIT, were collected during the release. Thermal neutron logs were taken periodically in the 12 glass wells. The chlorine atoms in the perchlorethelyne molecule have a large thermal neutron capture cross section so that the presence of PCE is manifested by a reduced count rate. In addition, a video camera was used at 8/23 and 9/22 in the same glass wells to identify the clay layers and also to follow the progress of the PCE which was dyed red (using floricyne???). Unfortunately, some time after 8/23 some of the glass wells were broken so that on 9/22 only wells g01-g04 could be logged. Both neutron and video data are presented in Figure 6 superimposed on the EIT results of Figure 4.

Neutron and video logs are important for understanding the distribution of PCE in the tank, however, direct comparison of these data and the EIT images must be made with caution because of two differences in what the data sample: (1) The video logs sample only immediately adjacent to a well whereas EIT samples away from the well a spatially average volume which is determined by the sampling interval (see Daily and Owen, 1991). There is also a smoothing of the image inherent in the inversion characterized by the resolution radius, or distance over which adjacent pixels are smoothed (see Description of 2D Algorithm). The resolution radius varies in response to sampling current density in the image plane, between 10 and 30 cm. In the central image where the DNAPL is imaged it is between 10 and 18 cm. (2) Some of the glass wells are as much as 1 meter from an image plane and therefore sample a different part of the tank. Third, during construction clay was unintentionally mixed with sand adjacent to the layers and very small amounts of clay will measurably change the electrical resistivity but will not be observable from the video log. We believe this mixing of small amounts of clay into surrounding sand is the principal reason the clay layers appear so non uniform in the EIT images.

The neutron logs suggest that the highest moisture level in the 100% bentonite layer is at is upper and lower surfaces. The clay layers may be wetting from the edges leaving the center dry during some of the experiment. Because of this process, the bentonite layers may exhibit electrical properties different from natural clays.

*Baseline EIT images, video and neutron logs*

Both the upper and lower pure bentonite layers, as delineated in the video logs, are centered on the EIT image of the layers. This is excellent agreement between these two measures of the clay layers. The EIT image of these layers is smoothed (smeared) during the inversion (the resolution radius is about 12 cm), making them appear somewhat thicker than seen in the video logs. Identification of the 1% bentonite was difficult in the video logs but where identified, it is included in the video log data. There is not evidence in the EIT images that the 1% bentonite layer can be distinguished from the pure bentonite layer.

Note that the upper clay layer was not identified in the video logs of wells g6 or g7 which were supposed to be adjacent to the layer. This is evidence that supports the EIT images which also suggest the layer was built shorter than planned. However, numerical modeling shows that some of this forshortening is an artifact of the inversion.

There is a small but significant neutron count rate in each well at the level of the clay layers which is due to the increased water content in the clay providing additional hydrogen to thermalize more neutrons. The position of the clay layers as determined by the neutron log is in good agreement with that imaged by EIT. Notice that the upper clay layer is also absent from the neutron logs in g6 and g7 supporting the EIT and video logs that layer did not extend all the way to the center of image plane L2-L3.

*EIT images of the spill and the video logs*

Dyed free product PCE is clearly visible in the video log pooled on the auquitards and residual held by capillarity in the sands. Along g5, g6 and g7 above the upper clay there are many short sections of PCE consistent with the remnants of a plume that has mostly drained from the sands which are probably small patches of PCE and so are below the detection threshold for EIT.

On the other hand, the pooled free product is identifiable in both the EIT and video data. There is, however, a systematic discrepancy between the EIT images and the video logs. EIT images show the pool as a resistive anomaly on top of the 1% bentonite layer while the video log shows it about 20 cm below this, sitting on the pure clay layer. We can't explain this difference as an error in registration of either EIT or the video logs because the position of the clay layers in both data sets match very well. As we shall see later, both the EIT images and neutron logs show the PCE on top of the 1% clay.

On August 23 the video data indicate PCE at g9 on the upper layer but not in g08 or g12 implying an isolated pocket of PCE on this layer. Since there is no resistive anomaly at this position in the EIT image we conclude that the accumulation is localized and not sampled by the EIT plane. By contrast, there appears to be a fairly continuous layer of PCE just above the lower clay since it is seen in all of the glass wells at this level. The same layer is seen in the EIT image of 08/21 but it is significant that the anomaly does not extend as far in either direction laterally.

*EIT images of the spill and the neutron logs*

The chlorinated solvent PCE can be seen in the thermal neutron logs because chlorine has a large capture cross section for thermal neutrons. The count rate plotted in Figure 5 will decrease in the

presence of PCE. This data should be a better indicator of PCE quantity than the video log because the probe integrates in a volume of 10 centimeters diameter (the well diameter is approximately 7 cm).

There is good overall agreement between the neutron data and the EIT images. For example, on the upper clay there is a depression of neutron count rate in g10, supporting the video data, but not in the other wells consistent with our earlier conclusion that this anomaly represents an isolated pocket outside the EIT image plane.

The neutron data even tracks the PCE in its movement down from the release point as it spills over the higher clay on its way to the lower layer (np5, np6 and np7 on 08/17; note that np stands for neutron probe surveys in g5) although the EIT image produces a much more intuitive picture (08/16, 08/17 and 08/18). At the lower clay there is also good agreement and especially important is that both data have the pool residing on top of the 1% bentonite layer. Remember that this is in contrast to the video data which located the pool about 20 cm lower on top of the pure bentonite layer. This discrepancy may result from the sampling differences between neutron, video and EIT. For example, the difference could be explained if, for some reason, a thin layer of PCE is able to move preferentially along the glass casing. This is consistent with relatively small changes in the neutron probe count extending below the pool to the pure clay layer but largest neutron depression remaining at the top of the 1% layer. Another explanation may be that electrical conduction in the sand is through the bulk pore water whereas in the 1% layer surface conduction along the clay particles interfaces may dominate. This means that the resistivity change when PCE displaces bulk pore water in the sands just above the 1% layer may be much larger than the change when PCE replaces bulk pore water within the 1% layer. Therefore, small amounts of PCE that move into the 1% layer, as indicated by the video logs, may be below our EIT sensitivity threshold.

Both neutron and video data confirm that the PCE pool extends laterally farther than the EIT anomaly. This discrepancy doesn't appear to be a sensitivity problem, but is a discrepancy which we which may be related to two observations that have not yet been mentioned. The first observation is that if Figure 5 were plotted on a scale showing the resistivity decreases relative to the baseline, we could see in each image a halo of low resistivity around the PCE

plume. The second observation is that when water is mixed with PCE and then allowed to separate, it has a resistivity about 7% lower than before it was mixed with the PCE. Some dissolved phase (impurity) may be causing this behavior and be the cause of the conductive halo around the PCE plume in the images. Where the free product plume is very thin, as might be expected near the outer edges, the small resistivity increase in the ERT images imposed by the free product may be overwhelmed by this resistivity decrease from dissolved phase.

## EIT of DNAPL without baseline data

The above results demonstrate that under some circumstances EIT can provide detailed underground images of free product PCE. Unfortunately, the circumstances severely limit the usefulness of the technique to times when baseline data is available (e.g., as might be possible while monitoring remediation). An important goal of this work is to provide images of DNAPL at a site which is contaminated before EIT data has been collected. This is a much more challenging case and the one encountered most commonly during site characterization.

Several methods might be used to image the PCE plume without the use of baseline data. We have tried both simple and subtle methods.

The simplest approach is to examine the absolute EIT images taken with the PCE in place, looking for an indicator to its presence such as a resistive anomaly immediately adjacent to the top of a confining layer. The rational for this approach is that since a chlorinated hydrocarbon can be identified near a borehole by thermal neutron measurements, ERT could be used to extrapolate our knowledge of its spatial distribution away from the well bore. Unfortunately, the relatively thin PCE layer is not resolved in the images since our pixels are 12.5 cm high and the PCE pool is likely less than that. In this circumstance EIT images the average resistivity in a volume defined by the resolution radius (Daily and Ramirez, 1995) and this will include the PCE layer as well as some of the water saturated sand above (which will be less resistive than the PCE layer) and clay beneath (which will be the least resistive component). The net result of adding the thin PCE layer is that the reconstructed boundary of the clay layer moves a little lower in the image but the effect does not allow identification of a distinct PCE anomaly in the absolute

image. We have also been unsuccessful at seeing the PCE pool in vertical gradient images.

More subtle methods include looking for changes in the electrical dispersion of PCE contaminated soils which might uniquely identify them. Following the lead of Olhoeft (1986, 1992), Trude *et al.* (1989) and Sadowski (1988) we want to image the electrical impedance phase during the DNAPL release. Unfortunately, direct measurement of phase using Zombie has produced relatively noisy data. As discussed earlier we have determined that better measure of phase is possible using the frequency effect. In an effort to image the spectral phase response of our sand-clay-DNAPL system and see the effect reported by Olhoeft (1986) and Vanhala (1996) we have examined the ratios of measured impedance magnitudes at two frequencies $|X(\omega_2)|\}/|X(\omega_2)|$ (see Eq. 9). Inversion of such ratios can be done as a crude perturbation technique where the quantity inverted is

$$(R_{h,DC})\,|X(\omega_2)|/|X(\omega_1)| \qquad (10)$$

where $R_{h,DC}$ is the transfer resistance magnitude calculated for a uniformly resistive finite element mesh of 1 ohm m assuming quasi static conditions and $|X(\omega_i)|$ is the impedance magnitude at $\omega_i$, which is a directly measured quantity. Reconstructions were done using Eq. 10 for both an upper frequency range ($\omega_2$=256 and $\omega_1$=64 Hz) and then again for a lower range ($\omega_2$=64 and $\omega_1$=1 Hz) with the reconstructed pixel values of the upper frequency range divided by the reconstructed pixel values of the lower frequency range to form the images in Figure 7.

Figure 7 shows a time series of the above described reconstructions from 0816 through 0914 (along with the reconstruction of the baseline resistivity for comparison). Note that these are not time comparison images but rather frequency comparison images so they do not require the baseline data. This type of processing is therefore possible from a site where data was collected only after the site was contaminated.

If the phase spectrum is constant with frequency between 1 Hz and 256 Hz the reconstructed pixel will have a value of 1.0. If the measured phase is larger at the higher frequencies (as suggested by Olhoeft (1986)), the reconstructed pixel will be larger than 1.0.

Conversely, if the phase is smaller at higher frequencies the pixel value will be smaller than 1.0.

We do not expect a phase spectral response in the uncontaminated case of 0816, baseline so that the variations in that image are likely data errors propagating through the code into the reconstruction. These variations are about 0.12 or 12%. Therefore, we are looking for a systematic change larger than 12% in or near the clay layers as DNAPL is added to the system. Successive images beginning with 0816, late (first image after DNAPL release) do show a systematic phase spectral response as DNAPL is added to the system. The trend is to larger values up to about 30%, loosely correlated to the lower clay layer (e.g., 0817, 0821 and 0824) and then a return to smaller values at later times (e.g., 0905 and 0914). This is the type of behavior we would expect if we were seeing a spectral phase response as reported by Olhoeft (1986) but with a magnitude comparable to the data errors. For this case we would expect a phase anomaly, normally centered on the plume, to be distorted by noise during the reconstruction.

## Summary and Conclusions

The electrical contrast between the sand and clay in the tank provided a target easily imaged using EIT. This fact alone is important to delineating free product DNAPL because the detailed characterization of aquitard layers identifies areas where contaminates might accumulate.

The time difference images of Figure 4 are the first EIT images of free product PCE in the subsurface and demonstrate that DNAPL can be imaged using the technique of looking for temporal changes. The reconstructions agree roughly with the neutron data. There is, however, an unexplained discrepancy between the video data and both the EIT and neutron log data. The ability to image free product DNAPL using EIT is important because such a technique could be used to monitor remediation of free product DNAPL at a level of detail that is not currently available.

The principle goal of this work is to determine if EIT can be used to image DNAPL without the benefit of baseline data. To realize this goal several schemes were tried using the EIT data from the OGI experiment. The most successful approach was to image the spectral phase response looking for increasing phase with contamination as

suggested by the laboratory data of Olhoeft (1986) and Vanhala (1996). The spectral reconstructions of subsurface electrical resistivity reported herein are the first of their kind and represent a significant technological achievement. The spectral phase images show a loose correlation between DNAPL accumulation at the top of the clay and increases in measured phase between 64 and 256 Hz compared to 1 and 64 Hz. Unfortunately, this phase dispersion was near the data measurement accuracy and so the reconstructions are not compelling. The reconstructions are, however consistent with the placement and shape of the PCE free product as imaged by ERT and as delineated by the neutron and video logs. The spectral phase images show anomalies increasing in magnitude as the PCE enters the formation, the anomalies growing laterally during the release, reaching a maximum extent near the end of the release and weakening after the release ended.

***Acknowledgments***

*We recognize the contributions of the following colleagues at Lawrence Livermore National Laboratory R. Newmark and M. McIntyre and the following colleagues at the Oregon Graduate Institute of Science and Technology Dr. Rick Johnson, W. Bagby and M. Perrot. The encouragement and technical advice from Aldo Mazella was important to the success of this project. We express our thanks to D. Roelant of BDM Federal for his assistance in initiating and managing this work. This work was sponsored by the CMST Program, Office of Technology Development, U. S. Department of Energy.*

*This study was performed under the auspices of the U.S. Department of Energy by Lawrence Livermore National Laboratory under contract W-7405-ENG-48.*

## REFERENCES

Bard, Y., *Nonlinear Parameter Estimation* (Academic Press, New York), pp. 111–113,1974.

Borner, F. D., J. R. Schopper and A. Weller, Evaluation of Transport and Storage Properties in Soil and Groundwater Zone from Induced Polarization Measurements, *Geoph. Prosp.*, **44**, 583-601, 1996.

Borner, F., M. Gruhne and J. Schon, Contamination indications derived from electrical properties in the low frequency range, *Geophysical Prospecting*, **41**, 83-98, 1993.

Considine, D. M., Van Nostrand's Scientific Encyclopedia, Sixth Edition, Van Nostrand Reinhold, Inc., 1983.

Daily, W. and A Ramirez, Electrical Resistance Tomography During In Situ Trichloroethylene Remediation at the Savannah River Site, *J. Applied Geophysics, 33*, 239-249, 1995.

Daily, W., A. Ramirez, D. LaBrecque and W. Barber, Electrical Resistance Tomography at the Oregon Graduate Institute Experiment, *J. of Applied Geophysics*, **33**, 227-237, 1995.

Huebner, K. H., and E. A. Thornton, *The Finite Element Method for Engineers* (Wiley, New York),1982.

Hohmann, G. W., 1988, "Numerical Modeling for Electromagnetic Methods in Geophysics," in Nabighian, M. N., Ed., Electromagnetic Methods in Geophysics, 1: Soc. Expl. Geophys., Invest. in Geophys., **no. 3**, 313–363 ,1986.

LaBrecque, D. J., *Cross-Borehole Resistivity Modeling and Model Fitting*, Ph.D. thesis, University of Utah, 1989.

LaBrecque, D. J., M. Miletto, W.Daily, A. Ramirez and E. Owen, The Effect of Noise on OCCAM's Inversion of Resistivity Tomography Data, Geophysics, **61**, 538-548, March-April 1996.

Olhoeft, G. R., Direct Detection of Hydrocarbon and Organic Chemicals with Ground Penetrating Radar and Complex Resistivity, *Proc. of the NWWA/API Conf. on Petroleum Hydrocarbons and Organic Chemicals in Ground Water--Prevention, Detection and Restoration*, 284-305, The Westin Galleria, Houston, Texas, 12-14 November 1986.

Olhoeft, G. R., Geophysical Detection of Hydrocarbon and Organic Chemical Contamination, *Symp. on the Application of Geophysics to Engineering and Environmental Problems*, R. S. Bell, ed., 587-595, April 26-29 1992.

Parasnis, D. S., *Mining Geophysics,* Elsevier Science Publishing Co., 1966

Ramirez, A. and W. Daily, Detection of leaks in underground storage tanks using electrical resistance methods: 1996 results, UCRL, Lawrence Livermore National Laboratory, October, 1996.

Ramirez, A., W. Daily, D. LaBrecque, E. Owen and D. Chestnut, Monitoring an Underground Steam Injection Process Using Electrical Resistance Tomography, *Water Resources Research*, **29**, no. 1, pp 73-88, 1993.

Sasaki, Y., "Resolution of Resistivity Tomography Inferred from Numerical Simulation," *Geophysical Prospecting* **40**, 453–463,1992.

Tikhonov, A. N. and Arsenin, V. Y., Solutions of ill-posed problems, ed. Fritz, J., John Wiley & Sonss, New York, 1977.

Trude, V. V., T. King and G. R. Olhoeft, Mapping Organic Contamination by Detection of Clay-Organic Processes, *Proc. Petrol Hydrocarbons and Org. Chem. in Ground Water: Prevent. Detect. and Restor. Conf.,* 627-640, Houston, AGWSE/NWWA/API, Dublin, OH, NWWA, Nov. 15-17, 1989.

Vanhala, H., Pollution Monitoring Using Spectral Induced Polarization (Spectral IP) Method, *Proc. Environmental and Engineering Geophysics Soc., European Section,* Mantes, France, 173-176, 2-5 September 1996.

Wannamaker, P. E., J. A. Stodt, and L. Rijo, *PW2D Finite Element Program for Solution of Magnetotelluric Responses of Two-Dimensional Earth Resistivity Structure,* DOE/SAN/12196-13, Univ. of Utah Research Institute, Earth Science Laboratory report ESL-158, 1987.

## Figure Captions

Figure 1. Laboratory measured impedance of uncontaminated and contaminated montmorillonite soil from Calcasieu Parrish landfill, Willow Springs, Louisiana. From Olhoeft (1986).

Figure 2. Block diagram of ZOMBIE, our data acquisition system.

Figure 3. EIT of resistor network. At the top is the network of 1000 ohm resistors used for the test. Each node at the periphery of the network is used for current injection or voltage measurement (i.e., an electrode location). On the left is the inversion of $(R_{h,DC})\ |X\ (\omega_2)|/|X\ (\omega_1)|$ where $R_{h,DC}$ is the transfer resistance magnitude calculated for a uniformly resistive finite element mesh of 1 ohm m assuming quasi static conditions and $|X\ (256)|$ is the measured impedance magnitude at 256 Hz, and $|X\ (1)|$ is the measured impedance magnitude at 1 Hz. On the right is the inversion of the same quantity but with four 1 $\mu$F capacitors added to the network as shown.

Figure 4. Construction of experimental tank and the EIT reconstruction of planes L1-L2-L3-L4. In the upper left is a plan view of borehole layout used for EIT and the glass wells. Below that are elevation views showing the relationship between the EIT arrays, glass wells and sand/clay layers. Superimposed on Section AA is the reconstruction of the baseline data from planes L1-L2-L3-L4.

Figure 5. EIT of the three coplanar tomographs L1-L2-L3-L4 at 1 Hz showing difference images of changes in resistivity between the baseline and subsequent times.

Figure 6. Thermal neutron and video logs superimposed on EIT images of Figure 5. Where they would overlap, neutron logs are offset from their projection on the ERT planes. Video log are coded so that red means dyed PCE, blue means 1% clay and green means 100% bentonite.

Figure 7. EIT reconstructions representing an increase in phase angle with increasing frequency. On the color bar a ratio of 1.0 represents no change in this estimate of the phase angle between the low and high frequency bands. A ratio of 1.25 represents an increase of 25%. The baseline image is shown for reference.

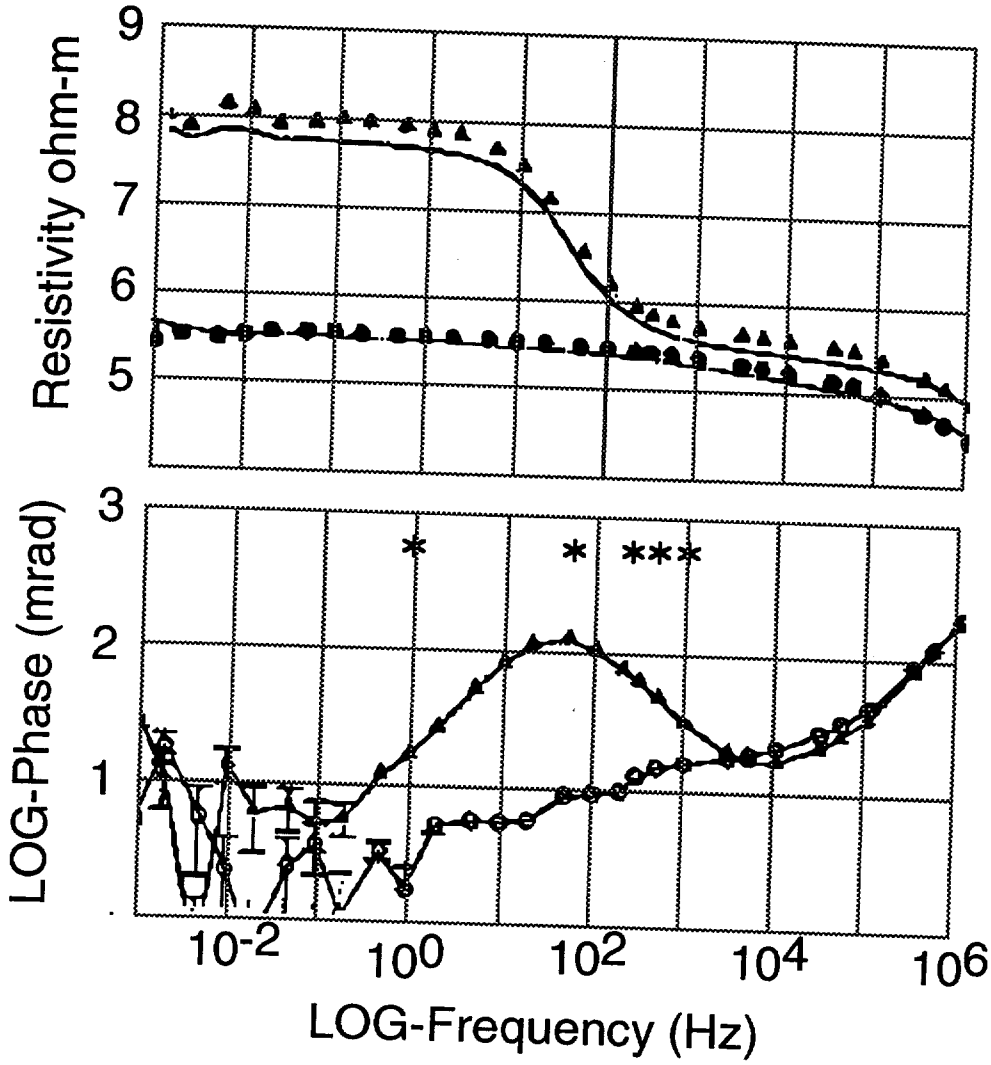
Resistivity ohm-m
9
8
7
6
5
LOG-Phase (mrad)
3
2
1
*
*
***
10-2
100
102
104
106
LOG-Frequency (Hz)
● uncontaminated
▲ contaminated
✳ frequencies at which LLNL data was collected

**Figure 1**

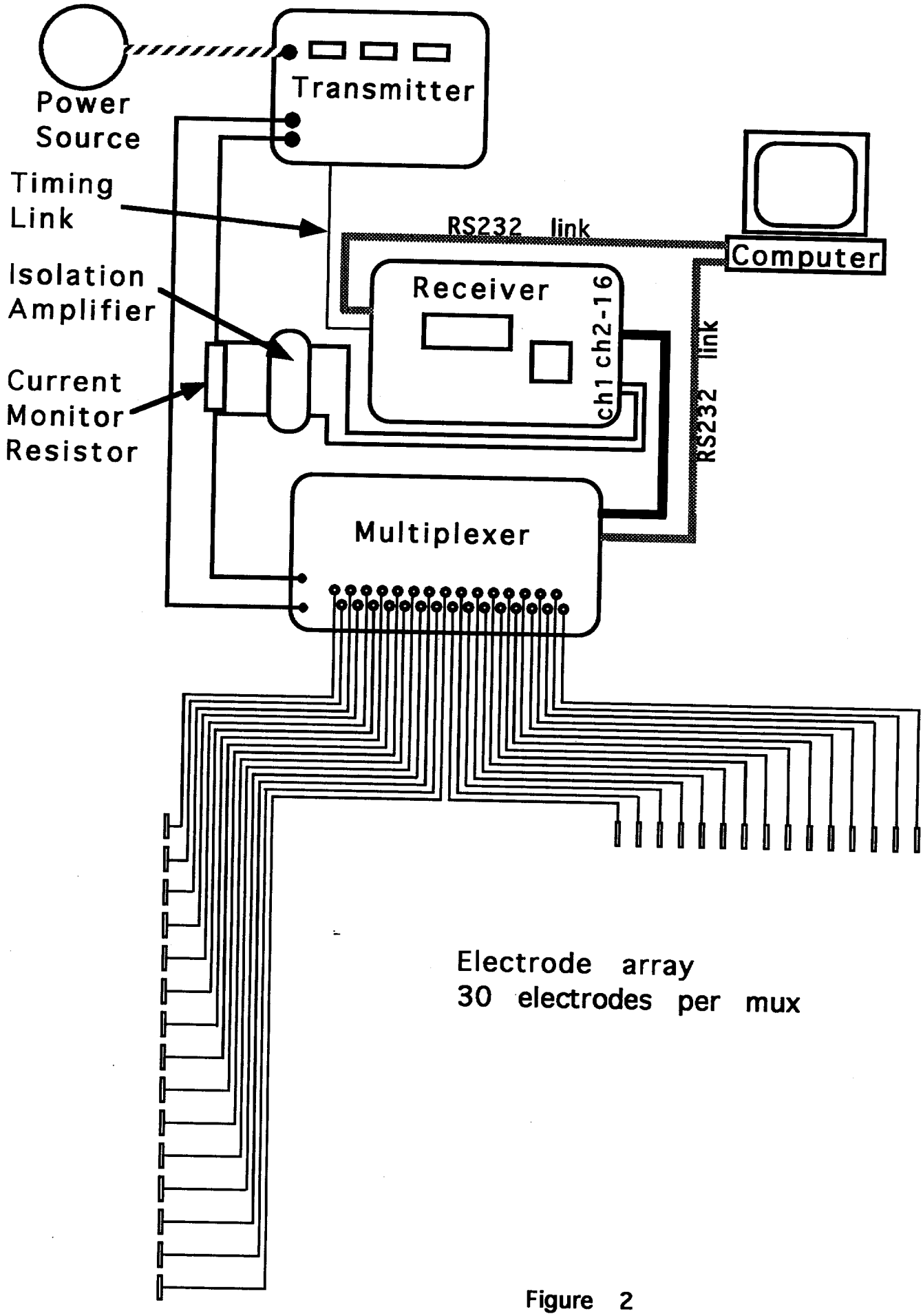
Power
Source
Transmitter
Timing
Link
RS232 link
Computer
Isolation
Amplifier
Receiver
ch1 ch2-16
RS232 link
Current
Monitor
Resistor
Multiplexer
Electrode array
30 electrodes per mux

Figure 2

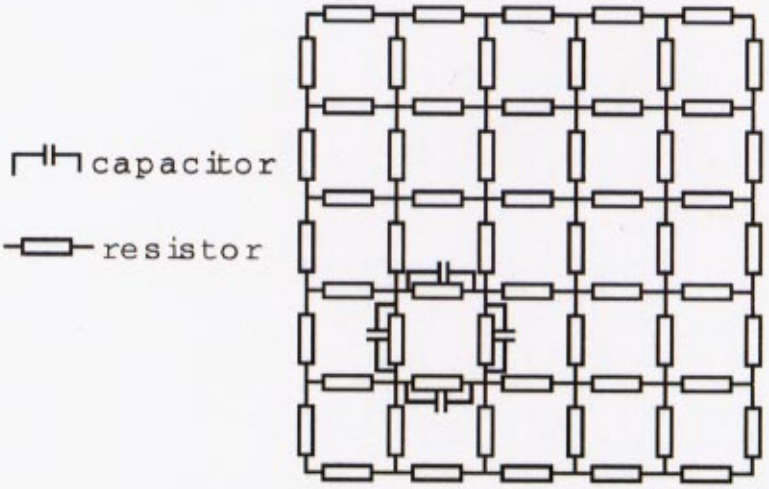


network of resistors and capacitors

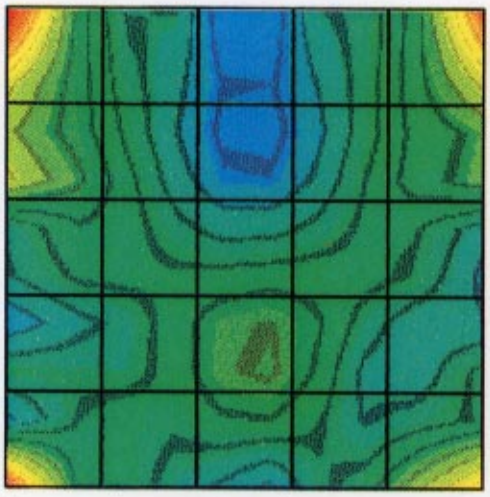

Inversion, Resistors only

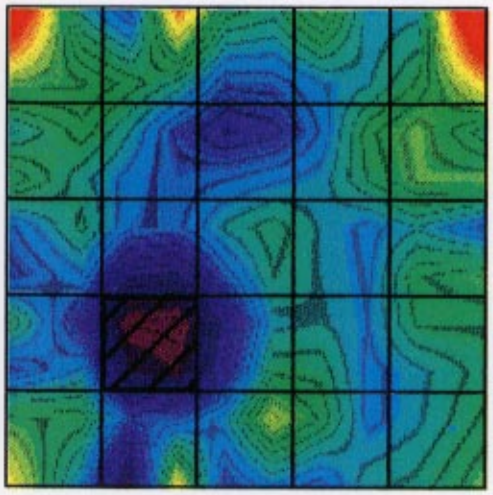

Inversion, Resistors and capacitors

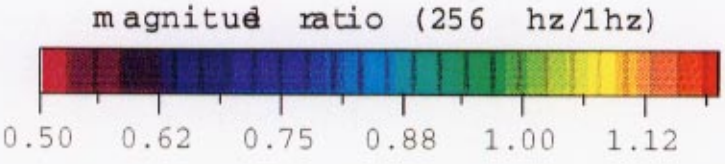


Figure 3

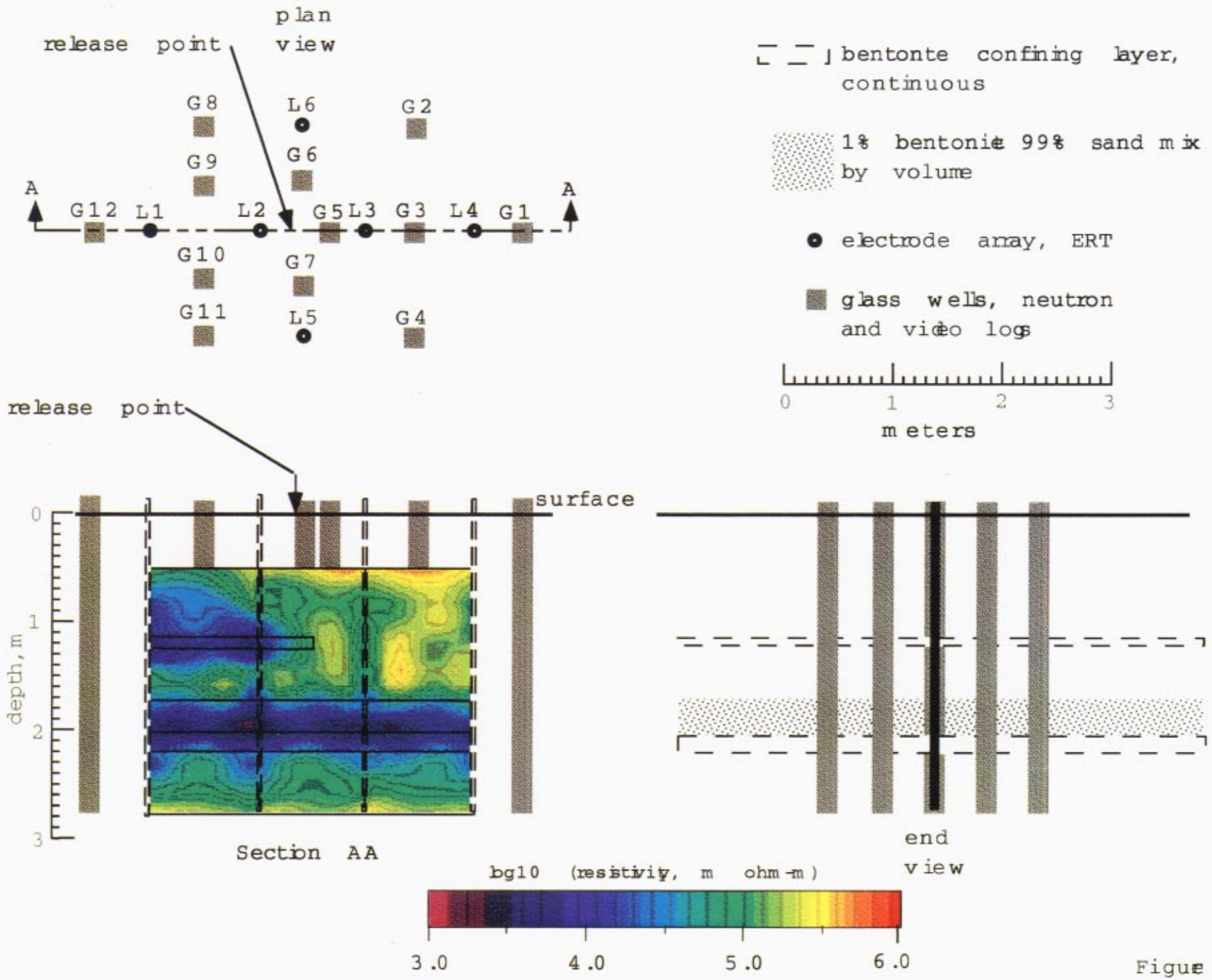
plan view
release point
G8
L6
G2
G9
G6
A
A
G12
L1
L2
G5
L3
G3
L4
G1
G10
G7
G11
L5
G4
bentonte confining layer, continuous
1% bentonie 99% sand mix by volume
electrode array, ERT
glass wells, neutron and video logs
0
1
2
3
meters
release point
surface
depth, m
0
1
2
3
Section AA
end view
bg10 (resistivity, m ohm-m)
3.0
4.0
5.0
6.0

Figure 4

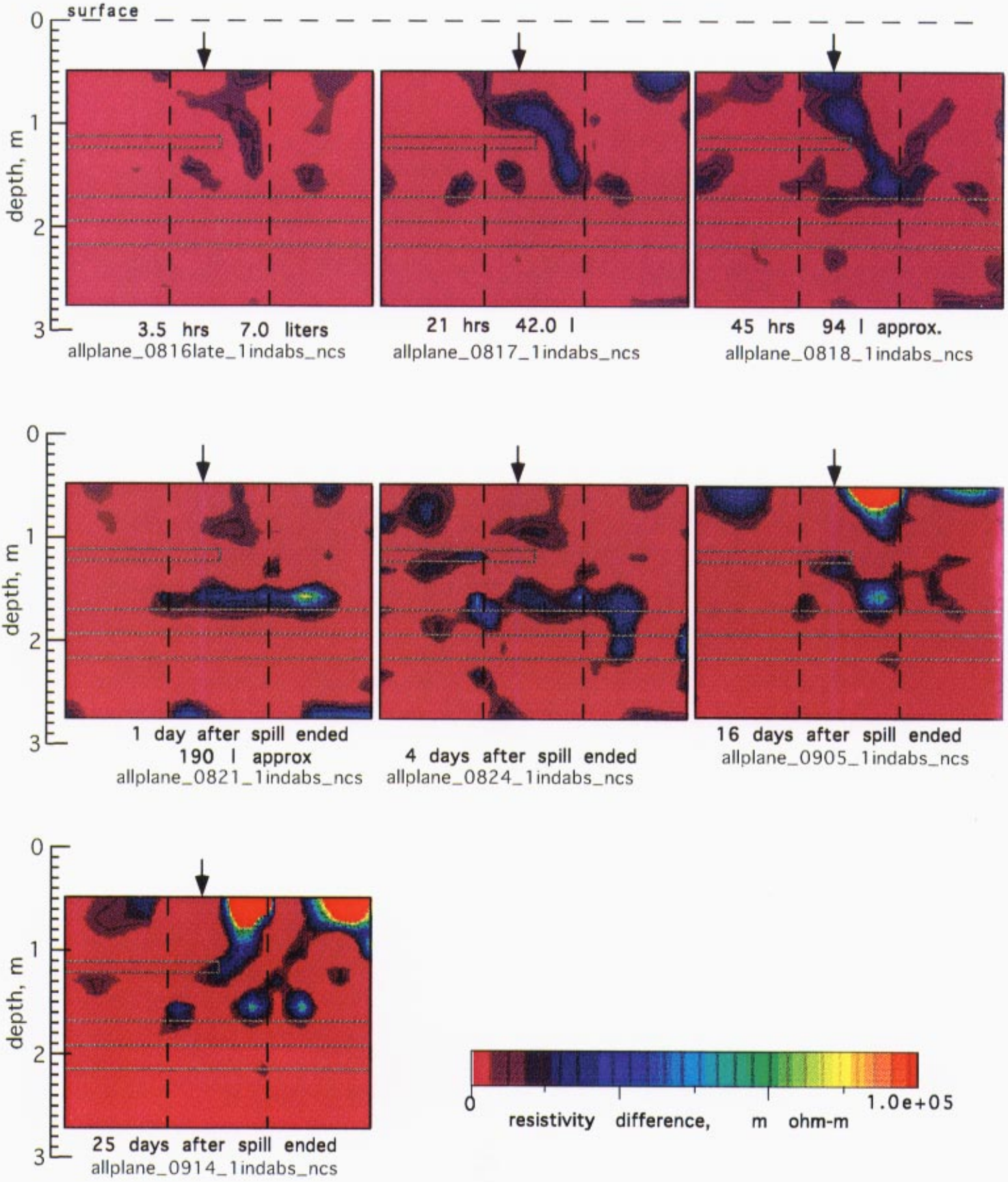
surface
depth, m
0
1
2
3
3.5 hrs 7.0 liters
allplane_0816late_1indabs_ncs
21 hrs 42.0 l
allplane_0817_1indabs_ncs
45 hrs 94 l approx.
allplane_0818_1indabs_ncs
1 day after spill ended
190 l approx
allplane_0821_1indabs_ncs
4 days after spill ended
allplane_0824_1indabs_ncs
16 days after spill ended
allplane_0905_1indabs_ncs
25 days after spill ended
allplane_0914_1indabs_ncs
0
1.0e+05
resistivity difference, m ohm-m

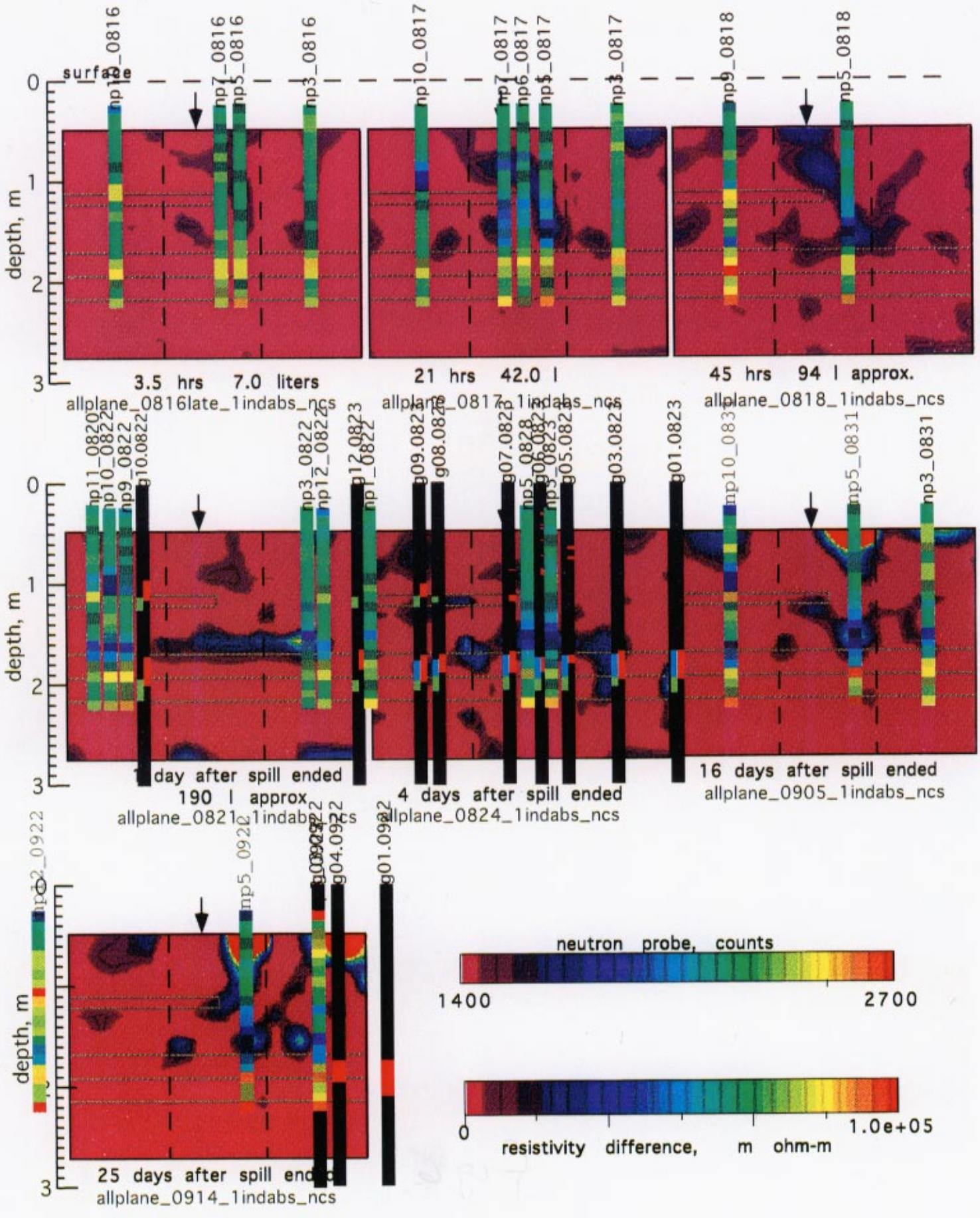
surface
depth, m
0
1
2
3
3.5 hrs 7.0 liters
allplane_0816late_1indabs_ncs
21 hrs 42.0 l
allplane_0817_1indabs_ncs
45 hrs 94 l approx.
allplane_0818_1indabs_ncs
1 day after spill ended
190 l approx.
allplane_0821_1indabs_ncs
4 days after spill ended
allplane_0824_1indabs_ncs
16 days after spill ended
allplane_0905_1indabs_ncs
25 days after spill ended
allplane_0914_1indabs_ncs
neutron probe, counts
1400
2700
0
1.0e+05
resistivity difference, m ohm-m

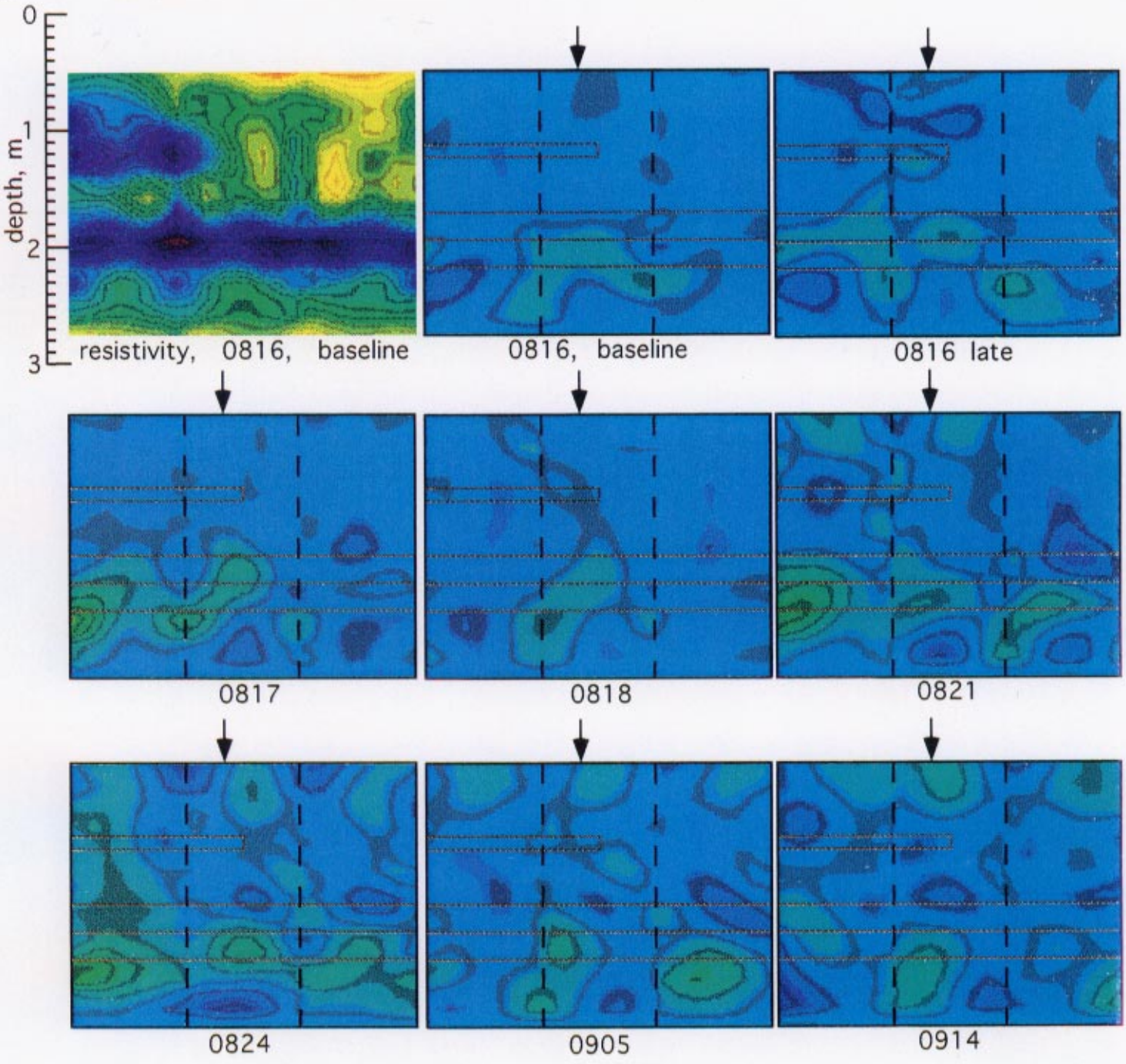
0
1
2
3
depth, m
resistivity, 0816, baseline
0816, baseline
0816 late
0817
0818
0821
0824
0905
0914

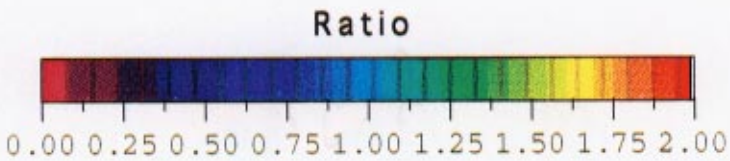
Ratio
0.00 0.25 0.50 0.75 1.00 1.25 1.50 1.75 2.00

*Technical Information Department* • **Lawrence Livermore National Laboratory**
**University of California • Livermore, California 94551**